International Conference on Applied Energy 2020
Dec. 1 - Dec. 10, 2020, Bangkok / Virtual
Paper ID: 208

Research on Flow-induced Vibration Response and Energy Conversion performance of Four-cylinder Acquatic Clean Energy Harvesting Device

Qunfeng Zou[1,2], Lin Ding[1,2,*], Tian Song[1,2], Li Zhang[1,2]
1. Key Laboratory of Low-grade Energy Utilization Technologies and Systems of Ministry of Education of China, Chongqing University, Chongqing, China
2. School of Energy and Power Engineering, Chongqing University, Chongqing, China
*Corresponding Author: Dr. Lin Ding, School of Energy and Power Engineering, Chongqing University, 174 Shazheng Street, Shapingba District, Chongqing, China, 400044; Phone: +86-23-65103101, E-mail: linding@cqu.edu.cn;

EnerarXiv-preprint

ABSTRACT

Flow induced vibrations (FIVs) of four tandem circular cylinders with roughness strips are numerically studied in Reynolds number range of 30,000≤*Re*≤100,000. The power conversion and FIV responses are discussed. The VIV initial branch, VIV upper branch, VIV to galloping transition, and galloping are clearly observed for first cylinder. The amplitude ratio curves of third and fourth cylinders show an upward trend and the branches of FIV are not obvious. Both the converted power and conversion efficiency of four cylinders are higher than those of one, two and three cylinders when 62,049≤*Re*≤90,000. The maximum total converted power reaches to 103W when *Re*=100,000.

Keywords: flow-induced vibration, galloping, power conversion, four circular cylinders

1. INTRODUCTION

Flow induced vibrations (FIVs) of cylinders, especially vortex induced vibration (VIV) and galloping are omnipresent in nature [1]. Vortex induced vibration (VIV) is a most common seen form of FIV and occurs in a broad velocity range. Galloping is another form of FIV and generated by the interruption of communication between the separated upper and lower flows. The vibration frequency and amplitude are important parameters that can quantify VIV and galloping. They can be influenced by the mass ratio [2], spring stiffness [3], damping, and incoming flow condition [4,5]. FIV can cause structural damage of many engineering applications, such as marine risers, tubes of heat exchangers, and large span bridges. Thus, most researches focus on suppressing FIV and many measures have been put forward [6,7,8].

On the other hand, energy can be harvested from the FIV. The Vortex Induced Vibration for Aquatic Clean Energy (VIVACE) Converter is a novel energy harvesting device from water [9]. The simplest form of energy converter designed by Bernitsas et al. [9] includes an elastically mounted circular cylinder. There are two ways to improve performance of the energy conversion by VIVACE converter. The first one is enhancing FIV of single cylinder. The Passive Turbulence Control (PTC) proposed by Chang et al. [10,11] can be an effective measure. According to the PTC-to-FIV map of a single circular cylinder [12], its location can affect the FIV profoundly. The application of PTC can enhance the FIV and further increases the energy extraction efficiency. The second way is using multiple cylinders in synergistic FIV [13,14].

It is concluded that the attack angle of incoming flow, reduced velocity, and the arrangement of cylinders almost determine the response of two cylinders [15,16]. Lin et al. [17] studied the flow induced vibrations of two circular cylinders arranged in tandem (*Re*=100) and found that the interaction between two circular cylinders would be enhanced at first and then decreased with the rising of spacing between them. Qin et al. [18] studied the FIV characters of two tandem circular cylinders with different frequencies ratios and they found a critical reduced velocity existed in the galloping regime, where the vibration amplitude of downstream cylinder increased sharply.

So far, it is not clear that whether the knowledge of two tandem circular cylinders can be extended to three or four circular cylinders. Shaaban and Mohany [19] numerically studied the FIVs of three circular cylinders and found that the arrangement of three circular cylinders with uneven spacing can trigger significant change in the flow characters. Chen et al. [20] numerically studied the

Selection and peer-review under responsibility of the scientific committee of the 12th Int. Conf. on Applied Energy (ICAE2020).
Copyright © 2020 ICAE

VIV of three tandem circular cylinders and elucidated the mechanism of wake-induced galloping.

In this work, the energy harvesting by FIVs of four circular cylinders with roughness strips in tandem is studied. The vibration characters and power conversion are analyzed. To validate the numerical results, the vibration responses are validated by the experiment results of Kim et al. [21].

2. PHYSICAL MODEL

Fig. 1 depicts the physical model, which is consisted of four vibration systems. Every vibration system consists of a rigid circular cylinder, a supporting spring, and the system damping (C) caused by friction. The diameter of each cylinder is D, and K represents the stiffness of the spring. Four cylinders are arranged in tandem and the distances between centers of two adjacent cylinders (d) are identically equal to 2.5D. The angle of PTC α_{PTC} is the angle measured from the forward stagnation point of a circular cylinder and equals to 30 °. The coverage of each sand-strip is 16 °[21]. Detailed parameters of the physical model can be seen in Table 1.

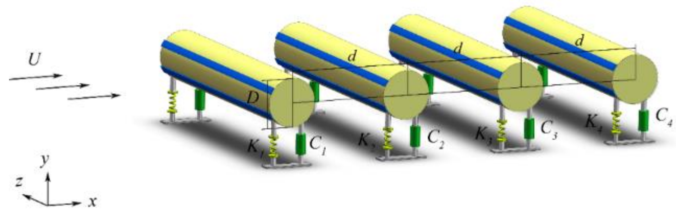

Fig. 1 Schematic diagram of the physical model

Table 1 Detailed parameters of the physical model

Item	Symbol	1st Cyl.	2nd Cyl.	3rd Cyl.	4th Cyl.
Diameter	D (m)	0.0889	0.0889	0.0889	0.0889
Length	L (m)	0.9144	0.9144	0.9144	0.9144
Vibration system mass	m_{osc} (kg)	9.5348	9.5852	9.5121	9.5756
Spring const.	K (N/m)	744.29	757.41	737.24	747.39
Damping ratio of system	ζ	0.021	0.020	0.017	0.168
Natural freq. in water	$f_{n,water}$ (Hz)	1.1135	1.1214	1.1090	1.1143
Mass ratio	m^*	1.68	1.69	1.68	1.69
Added mass coef.	C_a	1	1	1	1
Kinematic viscosity of water (m^2/s)	v	1.1389×10^{-6}			

3. COMPUTATIONAL METHOD

3.1 Governing equations

The open source software OpenFOAM was applied and in-house code has been developed. Two-dimensional and incompressible are considered. The incompressible Unsteady Reynolds-Averaged Navier-Stokes (URANS) equations in conjunction with the Spalart–Allmaras turbulence model are used to model the time-dependent viscous flow [22].

The governing equations are expressed as:

$$\frac{\partial U_i}{\partial x_i} = 0 \tag{1}$$

$$\frac{\partial U_i}{\partial t} + U_j \frac{\partial U_i}{\partial x_j} = -\frac{1}{\rho}\frac{\partial p}{\partial x_i} + \frac{\partial}{\partial x_j}(2\nu S_{ji} - \overline{u_j' u_i'}) \tag{2}$$

where x_i represents the Cartesian coordinate of i direction and U_i corresponds to the velocity component in i direction. The molecular kinematic viscosity is represented by v.

To model the vibration of four cylinders, the classical mass-spring-damper oscillator model is adopted

$$m_{osc}\ddot{y} + C\dot{y} + Ky = \mathrm{F}_{fluid,y}(t) \tag{3}$$

where m_{osc} is the total vibrating mass of every vibration system, y represents the oscillator displacement in the y-direction. $F_{fluid,y}$ (t) is the fluid force in the y direction.

The power converted by a cylinder from the hydrokinetic energy in the flow is calculated by

$$P_{convert} = \frac{1}{T_{osc}}\int_0^{T_{osc}} F_{fluid,y}(t)\dot{y}dt + \frac{1}{T_{osc}}\int_0^{A_{peaks}} Kydy \tag{4}$$

Inserting the left side of Equ. (3) into Equ. (4)

$$P_{convert} = \frac{1}{T_{osc}}\int_0^{T_{osc}} [m_{osc}\ddot{y} + C\dot{y} + Ky]\dot{y}dt + \frac{1}{T_{osc}}\int_0^{A_{peaks}} Kydy \tag{5}$$

The vibration of a cylinder in FIV can be assumed as a sinusoidal response, and the amplitude and its differential can be expressed as

$$y = A_{peaks}\sin(2\pi f_{osc} t) \tag{6}$$

Then, Equ. (14) can be rewritten as

$$P_{convert} = 2\pi^2 f_{osc}^2 A_{peaks}^2 C + \frac{1}{2}KA_{peaks}^2 f_{osc} \tag{7}$$

For multiple cylinders, the total power converted by cylinders is the sum of that of each cylinder, and can be calculated by

$$P_{convert,total} = \sum_i^n P_{convert,i} \tag{8}$$

The power in the fluid can be calculated as

$$P_{fluid} = \frac{1}{2}\rho U^3 (2A_{peaks} + D)L \tag{9}$$

EnerarXiv preprint

Copyright © 2020 ICAE

The power conversion efficiency of multiple cylinders is defined as

$$\eta_{convert}(\%) = \frac{P_{convert,total}}{P_{fluid}} \times 100 \qquad (10)$$

3.2 *Integration scheme*

To deal with the gradient, divergence and Laplacian terms in governing equations, a second order Gauss integration with a linear interpolation for the unknown face-centered values is adopted. The mixed explicit and implicit time integration scheme with second-order accuracy has been adopted by a lot of scholars [24,25].

3.3 *Computational domain and grid generation*

As shown in Fig. 2, the size of the computational domain is 57.5D×9D. The downstream and upstream lengths are l_{up},=l_{down}=25D. Zero velocity gradient is applied in outflow boundary. The cylinders surfaces is set as moving wall. The computational domain is divided into: (a) the eddy viscosity from the inflow boundary to first cylinder's center is set as zero, (b) the eddy viscosity from the center of first cylinder to the outflow boundary is set as the molecular eddy viscosity.

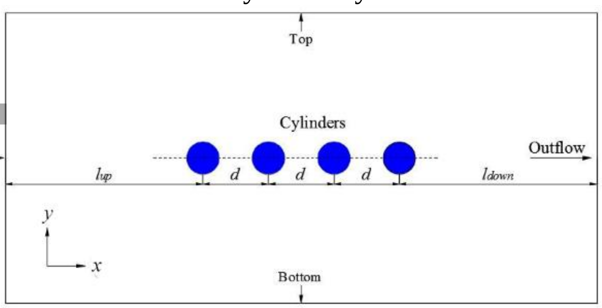

Fig. 2 Computational domain

The grid sensitivity study was done for the stationary PTC-cylinders. Three grid densities for the subdomain around each cylinder are: coarse (180×40), medium (240×70), and fine (360×100). The results of grid resolution study can be seen in Table 2. The medium grid resolution is selected in simulation after the comprehensive comparison of output parameters. A close-up of the medium size grid is depicted in Fig. 3(a), and a close-up of the medium grid for four cylinders in FIV can be seen in Fig. 3(b).

Table 2 Grid resolution study for 4 cylinders system (Re=3×10^4)

Grid (Central square)	cylinder	C_D	C_L	S_t
Coarse (180×40)	1st	1.505	1.199	0.214
	2nd	0.550	1.549	0.214
	3rd	0.158	1.100	0.213
	4th	0.215	0.324	0.213
Medium (240×70)	1st	1.499	1.213	0.213
	2nd	0.547	1.554	0.213
	3rd	0.153	1.110	0.213
	4th	0.209	0.324	0.213
Fine (360×100)	1st	1.490	1.220	0.213
	2nd	0.545	1.560	0.213
	3rd	0.155	1.119	0.213
	4th	0.210	0.322	0.213

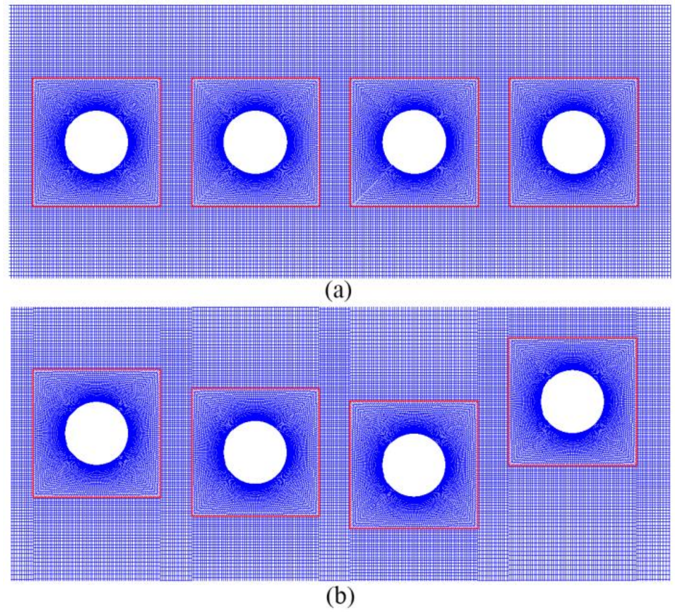

Fig. 3 Close-up of the grid for four cylinders

4. RESULTS AND DISCUSSION

4.1 *Amplitude response*

The Reynolds numbers are between 3×10^4 and 10^5 and fall in the high-lift TrSL3 regime [26]. To validate the numerical results, the parameters in simulation are identical to that of experiment conducted in the LTFSW channel of MRELab [27]. And the vibration amplitudes and vibration frequency ratios of four cylinders are compared with the experiment results of Kim et al. [21]. Fig. 4 shows the amplitude ratio curves of four cylinders. The amplitudes are non-dimensionalized by the diameter of the cylinder. As can be seen in Fig. 4, the numerical results follow the basic trend of the experimental data. Four branches can be observed in both numerical simulation and experiment, they are:

Copyright © 2020 ICAE
EnerarXiv-preprint

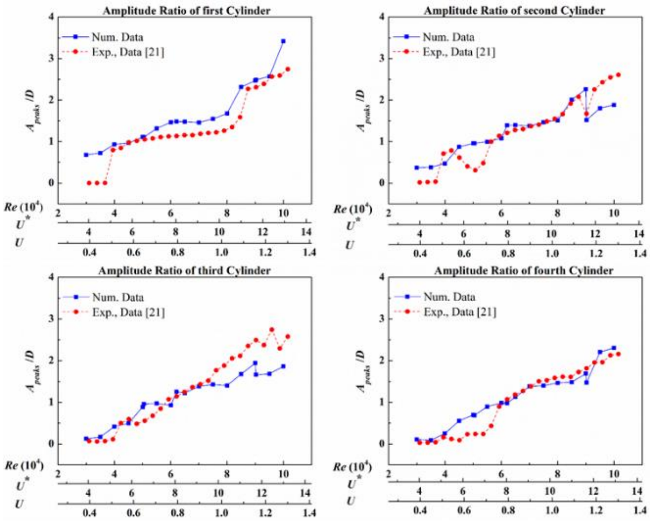

Fig. 4 Amplitude ratios of four cylinders in tandem

(1) The VIV initial branch: The first cylinder is in the initial branch of VIV when $U^*\leq5.18$ ($Re\leq40{,}000$). The first cylinder in numerical simulation starts to vibrate earlier ($U^*=3.88$) than that in experiments ($U^*=5.11$). Because the classical linear viscous damping model is adopted in CFD study, but the physical damping model in experiments is much more complex due to the application of the V_{CK} system [28]. The second cylinder in numerical simulation also starts to vibrate ($U^*=3.86$, $Re=3\times10^4$) earlier than that in experiments ($U^*=5.07$, $Re=39{,}486$). For the third cylinder, the amplitudes of third cylinder in simulation are still slight larger than that of experiment. For the fourth cylinder, the amplitudes of the CFD results agree well with that of experiment.

(2) The VIV upper branch: For the first cylinder, the region between $U^*=5.18$ ($Re=4\times10^4$) and $U^*=10.35$ ($Re=80{,}000$) is the upper branch of VIV. The amplitude ratios in simulation and experiment increase with the rising of U^*. For second cylinder, the numerical results agree well with the experimental data in VIV upper branch ($5.14\leq U^*\leq10.28$, $4\times10^4\leq Re\leq8\times10^4$), and the amplitudes of second cylinder increase with the rising of *Re*. For third and fourth cylinder, the amplitudes show an upward trend in numerical simulation. However, when $U^*=6.93$ ($Re=53{,}588$), the amplitude of fourth cylinder starts to increase sharply in experiment, which means the transition from initial branch to upper branch.

(3) Transition region: $10.35\leq U^*\leq11.65$ ($8\times10^4\leq Re\leq9\times10^4$), first cylinder is in the region of transition from VIV to galloping. The amplitudes increase fast in both numerical simulation and experiment. For second cylinder, the drop of the amplitudes is observed. This is mainly caused by the instability of cylinder in the transition phase of FIV. For third and fourth cylinders, the transition is not obvious, but the drop of amplitude ($Re=90{,}254$) can be observed in simulation.

(4) Galloping: The first cylinder is in galloping when $U^*>11.65$ ($Re>9\times10^4$). And the maximum amplitude in simulation reaches 3.5*D*, which is far higher than the 2.8*D* in experiment. Because the first cylinder has reached the position of the stop valve in the LTFSW channel in experiment [21]. Due to the exist of first cylinder, the amplitudes of three downstream cylinders are lower than those of first cylinder in this region.

4.2 Frequency response

The vibration frequency of each cylinder is non-dimensionalized by the natural frequency in still water, $f_{n,water}$. The frequency ratio curves of four cylinders are shown in Fig. 5.

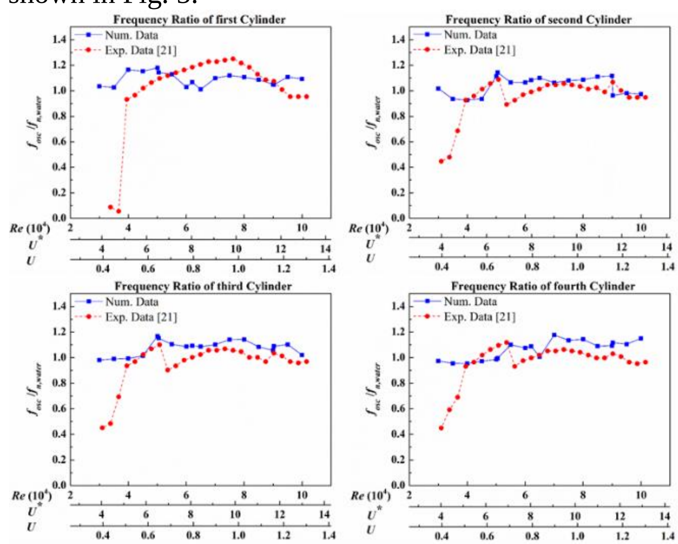

Fig. 5 Frequency ratios of four cylinders in tandem

In VIV initial branch, the frequency ratios of four cylinders in numerical simulation are all around the natural frequencies in water. The frequency ratios of four cylinders in experiment all jump to nearly 1.0 when $Re=4\times10^4$. In VIV upper branch of 1st cylinder, the frequency ratios in simulation are over-predicted. For other three cylinders, most of the frequency ratios of CFD results are slightly larger than those in experiment. During the transition from VIV to galloping, the vibration frequencies of 1st cylinder in both simulation and experiment drop with the rising of U^*. For 2nd cylinder, the decrease of the vibration frequencies in both numerical simulation and experiment can also be observed when $U^*=11.65$ ($Re=9\times10^4$). In galloping region ($U^*>11.65$), the vibration frequencies of 1st and 2nd cylinders in both numerical simulation and experiment tend to be stable. For the vibration frequencies of third and fourth cylinders, there are different levels of fluctuations when $U^*>11.65$.

4.3 Converted power

EnerarXiv preprint

 Copyright © 2020 ICAE

Fig. 6(a) depicts the total power converted by four cylinders. On the whole, the total converted power for all cases rise with the rising of U^* and the number of cylinders. When the Re<50,468, the total converted power is slightly lower than that of three cylinders [29], but larger than that of single cylinder [11]. For $5.5\times10^4 \leq Re \leq 9\times10^4$, the total converted power of four cylinders is larger than those of other cases and increase rapidly when $Re \geq 8\times10^4$. When Re=90,254, the total converted power of four cylinders suddenly drops and becomes slightly lower than that of three cylinders. When $Re=10^5$, four cylinders are all in galloping and the total converted power of four cylinders reaches to 103 W, which is the largest value in the studied Re range.

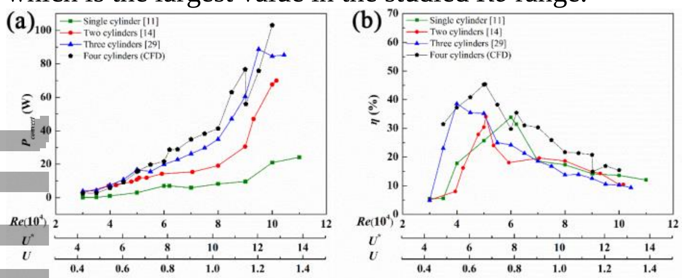

Fig. 6 (a) The total power converted by different numbers of cylinders, (b) The power conversion efficiencies corresponding to different numbers of cylinders

Fig. 6(b) shows the power conversion efficiencies (η) of one, two, three and four circular cylinders. For the four cases, the value of η all rise to a peak value and then decline with the rising of U^*. The value of $(\eta)_{max}$ increase with the rising of number of cylinders. When Re=50,408, the case of four cylinders has the highest value of η, thus 45.36%. The value of η for four cylinders are the highest among four cases and drops with the rising of Re when $Re \geq 4.5\times10^4$, the value of η for four cylinders is slightly lower than that of single cylinder. It can be concluded that four cylinders in tandem have advantages in both the total converted power and power conversion efficiency when 62,049 $\leq Re \leq$90,000.

5. CONCLUSIONS

From above discussion, the following conclusions can be drawn.

(1) The numerical method employed in this work is effective and the amplitudes and frequencies of four cylinders in simulation correspond well with the experimental data.

(2) The VIV initial branch, VIV upper branch, VIV to galloping transition, and galloping are all clearly observed for the first cylinder. Because of the influence of two upstream cylinders, the amplitude ratio curves of third and fourth cylinders show an upward trend.

(3) After entering VIV upper branch, the frequencies of four cylinders with roughness strips in tandem always maintain around the natural frequency of each cylinder in water. During the transition from VIV to galloping, the decrease of the vibration frequencies of first and second cylinders can be observed in both simulation and experiment.

(4) The total power converted by four cylinders increases with the reduced velocity (Reynolds number) increasing. The power conversion efficiency increases to a peak value, and then declines with reduced velocity increasing. The maximum power conversion efficiency of 45.36% can be captured when Re=50,408. When 62,049$\leq Re \leq$90,000, the total converted power and power conversion efficiency of four cylinders are higher than those of one, two and three circular cylinders with roughness strips.

ACKNOWLEDGEMENT

The authors gratefully acknowledge the support from the National Natural Science Foundation of China (Grant No.51776021), Natural Science Foundation of Chongqing, China (Grant No. cstc2020jcyj-msxmX0813), and Fundamental Research Funds for the Central Universities (Grant No. 2020CDJ-LHZZ-045). The authors also acknowledge the help from VIVACE group of Marine Renewable Energy Laboratory of the University of Michigan, and special thanks to Professor M.M. Bernitsas and Dr. Eun Soo Kim.

REFERENCE

[1] Sun W, Zhao D, Tan T, Yan Z, Low X. Low velocity water flow energy harvesting using vortex induced vibration and galloping. Appl. Energ 2019;251:113392.

[2] Chung MH. On characteristics of two-degree-of-freedom vortex induced vibration of two low-mass circular cylinders in proximity at low Reynolds number. Int. J. Heat Fluid Flow 2017;65:220-245.

[3] Han XX, Lin W, Tang YH, Zhao CB, Sammut K. Effects of natural frequency ratio on vortex-induced vibration of a cylindrical structure. Comput. Fluids 2015;110:62-76.

[4] Shaharuddin NMR, Mat Darus IZ. Experimental study of vortex-induced vibrations of flexibly mounted cylinder in circulating water tunnel. Acta Mech 2015;226:3795-3806.

[5] Pearcey T, Zhao M, Xiang Y, Liu M. Vibration of two elastically mounted cylinders of different diameters in oscillatory flow. Appl. Ocean Res 2017;69:173-190.

[6] Wang CL, Tang H, Yu SCM, Duan F. Control of vortex-induced vibration using a pair of synthetic jets: Influence of active lock-on. Phys. Fluids 2017;29:083602.

[7] Wang J, Geng L, Ding L, Zhu H, Yurchenko D. The state-of-the-art review on energy harvesting of flow-induced vibrations, Appl. Energ 2020;267: 114902.

[8] Zhang H, Liu MK, Han Y, Gui MY, Li J, Chen ZH. Suppression mechanism of two-degree-of-freedom

EnerarXiv preprint

Copyright © 2020 ICAE

vortex-induced vibration by Lorentz forces in the uniform flow. Comput. Fluids 2017;159:112-122.
[9] Bernitsas MM. VIVACE (Vortex Induced Vibration Aquatic Clean Energy) : A new concept in generation of clean and renewable energy from fluid flow. J. Offshore Mech. Arct. Eng 2008;130:041101.
[10] Chang CC, Kumar RA, Bernitsas MM. VIV and galloping of single circular cylinder with surface roughness at $3.0\times10^4 \le Re \le 1.2\times10^5$. Ocean Eng 2011;38:1713-1732.
[11] Ding L, Zhang L, Bernitsas MM, Chang CC. Numerical simulation and experimental validation for energy harvesting of single-cylinder VIVACE converter with passive turbulence control. Renew. Energy 2016;85:1246-1259.
[12] Park H, Kim ES, Bernitsas MM. Sensitivity to zone covering of the map of passive turbulence control to flow-induced motions for a circular cylinder at $30{,}000 \le Re \le 120{,}000$. J. Offshore Mech. Arct. Eng. Trans. ASME 2017;139:021802.
[13] Sun H, Ma CH, Kim ES, Nowakowski G, Mauer E, Bernitsas MM. Hydrokinetic energy conversion by two rough tandem-cylinders in flow induced motions: Effect of spacing and stiffness. Renew. Energy 2017;107:61-80.
[14] Kim ES, Bernitsas MM. Performance prediction of horizontal hydrokinetic energy converter using multiple-cylinder synergy in flow induced motion. Appl. Energy 2016;170:92-100.
[15] Mysa RC, Kaboudian A, Jaiman RK. On the origin of wake-induced vibration in two tandem circular cylinders at low Reynolds number, J. Fluid Struct 2016;61:76-98.
[16] Tu JH, Zhou D, Bao Y, Ma J, Lu JB, Han ZL. Flow-induced vibrations of two circular cylinders in tandem with shear flow at low Reynolds number. J. Fluid Struct 2016;59:224-251.
[17] Lin JZ, Jiang RJ, Chen ZL, Ku XK. Poiseuille flow-induced vibrations of two cylinders in tandem. J. Fluid Struct 2013;40:70-85.
[18] Qin B, Alam MM, Ji CN, Liu Y, Xu SJ. Flow-induced vibrations of two cylinders of different natural frequencies. Ocean Eng 2018;155:189-200.
[19] Shaaban M, Mohany A. Flow-induced vibration of three unevenly spaced in-line cylinders in cross-flow. J. Fluid Struct 2018;76:367-383.
[20] Chen WL, Ji CN, Williams J, Xu D, Yang LH, Cui YT. Vortex-induced vibrations of three tandem cylinders in laminar cross-flow: Vibration response and galloping mechanism. J. Fluid Struct 2018;78:215-238.
[21] Kim ES, Bernitsas MM, Kumar RA. Multicylinder flow-induced motions: Enhancement by passive turbulence control at $28{,}000<Re<120{,}000$. J. Offshore Mech. Arct. Eng. Trans. ASME 2013;135:021802.
[22] Spalart PR, Allmaras SR. A one-equation turbulence model for aerodynamic flows. Recherch é Aerospatiale 1994;1:5-21.
[23] Travin A, Shur M, Strelets M, Spalart P. Detached-eddy simulations past a circular cylinder. Flow Turbul. Combust 2000;63:293-313.
[24] Ding L, Bernitsas MM, Kim ES. 2-D URANS vs. experiments of flow induced motions of two circular cylinders in tandem with passive turbulence control for $30{,}000<Re<105{,}000$. Ocean Eng 2013;72:429-440.
[25] Wu W, Bernitsas MM, Maki K. RANS simulation versus experiments of flow induced motion of circular cylinder with passive turbulence control at $35{,}000<Re<130{,}000$. J. Offshore Mech. Arct. Eng. Trans. ASME 2014;136:041802.
[26] Zdravkovich MM, Bearman PW. Flow around circular cylinders—Volume 1: Fundamentals. J. Fluid Eng 1998;120:105-106.
[27] Bernitsas MM, Ben-Simon Y, Raghavan Y, Garcia EM. The VIVACE Converter: Model tests at high damping and Reynolds number around 10^5. J. Offshore Mech. Arct. Eng-Trans. ASME 2009;131:01102.
[28] Lee JH, Xiros N, Bernitsas MM. Virtual damper–spring system for VIV experiments and hydrokinetic energy conversion. Ocean Eng 2011;38:732-747.
[29] Ding L, Zou QF, Zhang L, Wang HB. Research on flow-induced vibration and energy harvesting of three circular cylinders with roughness strips in tandem. Energies 2018;11:2977.

EnergyArXiv preprint

Copyright © 2020 ICAE